Inorganics **2014**, *2*, 16-28; doi:10.3390/inorganics2010016

OPEN ACCESS

inorganics

ISSN 2304-6740

www.mdpi.com/journal/inorganics

Article

Investigation into the Incorporation of Phosphate into $BaCe_{1-y}A_yO_{3-y/2}$ (A = Y, Yb, In)

Alaric D. Smith and Peter R. Slater

School of Chemistry, University of Birmingham, Birmingham B15 2TT, UK;
E-Mails: axs159@bham.ac.uk (A.D.S.); p.r.slater@bham.ac.uk (P.R.S); Tel.: +44-121-414-8906

Received: 26 November 2013; in revised form: 23 January 2014 / Accepted: 24 January 2014 / Published: 29 January 2014

Abstract: In this paper we examine the effect of doping phosphate into $BaCe_{1-y}A_yO_{3-y/2}$ (A = Y, Yb, In). The samples were analysed through a combination of X-ray diffraction, TGA, Raman spectroscopy and conductivity measurements. The results showed that phosphate could be incorporated into this system up to the 10% doping level, although this required an increased Y/Yb/In content, e.g., $BaCe_{0.6}(Y/In/Yb)_{0.3}P_{0.1}O_{2.9}$. The phosphate doping was, however, shown to lead to a decrease in conductivity; although at low phosphate levels high conductivities were still observed, e.g., for $BaCe_{0.65}Y_{0.3}P_{0.05}O_{2.875}$, $\sigma = 4.3 \times 10^{-3}$ S cm^{-1} at 600 °C in wet N_2. In terms of the effect of phosphate incorporation on the CO_2 stability, it was shown to lead to a small improvement for the In containing samples, whereas the yttrium doped compositions showed no change in CO_2 stability.

Keywords: perovskite; proton conductor; phosphate; cerate; oxyanions

1. Introduction

There has been considerable research carried out into perovskite-related materials for use as electrode and electrolyte materials in solid oxide fuel cells. Traditional doping strategies to optimize electrolyte materials have involved doping a cation with a similar sized aliovalent cation e.g., $LaGaO_3$, doped with Sr on the La site and Mg on the Ga site [1–3]. This doping strategy introduces oxide ion vacancies into the lattice, which allows the conduction of oxide ions or the incorporation of water to facilitate proton conduction [1,3,4]. $Ba(Ce/Zr)O_3$ doped with Y on the Ce/Zr site has attracted considerable interest as a high temperature proton conductor in wet atmospheres, due to water incorporation into the oxide ion vacancies according to Equation 1 [5–7].

$$v_O^{\bullet\bullet} + O_O + H_2O \leftrightarrow 2\ OH_O^{\bullet} \quad (1)$$

While Y doped $BaCeO_3$ shows very high proton conductivity a major drawback with this system is its instability towards CO_2, forming $BaCO_3$ at the operating temperatures of solid oxide fuel cells (500–800 °C) [8]. Y doped $BaZrO_3$ can be used as an alternative electrolyte, as it displays improved CO_2 stability, however this system typically exhibits a high grain boundary resistivity [9,10]. Recently there has been considerable interest in strategies to increase the grain size in Y doped $BaZrO_3$, through the use of sintering aids, or in the preparation of mixed Zr/Ce systems to try and resolve these issues [11,12]. Another system that has attracted a significant attention is the brownmillerite structured $Ba_2In_2O_5$ [13–16]. This system has a high level of oxygen vacancies and this leads to oxygen vacancy ordering such that there are alternating layers of octahedrally and tetrahedrally coordinated In, leading to a comparatively low ionic conductivity. Doping this system with higher charge aliovalent cations of similar size (e.g., Zr^{4+} and Ti^{4+} for In^{3+}) has been shown to introduce disorder onto the oxide lattice, and hence improve the conductivity. An alternative strategy developed in our group to optimize the conductivity of $Ba_2In_2O_5$ has been to introduce oxyanions (MO_4^{n-}; M = Si, P, S), where the central cation of the oxyanion is located onto the perovskite cation B site, and the oxide ions of this group fill four of the available six oxide ion sites surrounding it (albeit displaced so as to achieve the tetrahedral coordination of the oxyanion group). This strategy was found to enhance oxide ion conduction by creating disorder on the oxide ion sublattice. Further enhancements in the conductivity were observed in wet atmospheres leading to water incorporation and a protonic contribution to the conductivity. Oxyanion doping was also shown to improve the stability of the system to CO_2 atmospheres attributed to a reduction of the basicity of the system with these acidic dopants [17–20]. This strategy was then extended to $Ba_2Sc_2O_5$ and $Ba_2Sc_{2-y}Ga_yO_5$, with phosphate and sulfate doping showing improved stability to CO_2 [21,22]. In this paper, we extend this oxyanion doping strategy to In, Y, Yb doped $BaCeO_3$ with the hope of improving the CO_2 stability and analyzing the effect on the conductivity. As noted previously by Soares *et al.*, the effect of P additions in $BaCeO_3$ is also of relevance, since phosphate esters have been used as dispersants to prevent nanoparticle agglomeration in the preparation of related perovskite materials [23]. In this previous work, Soares *et al.* examined $(1 - x)BaY_{0.15}Zr_{0.85}O_{2.925}{:}xP_2O_5$ mixtures, and observed the presence of $Ba_3(PO_4)_2$ impurities, and had a negative effect on the conductivity. The addition of P_2O_5 to an as-prepared single phase $BaY_{0.15}Zr_{0.85}O_{2.925}$ perovskite, however meant that the examined compositions were effectively A site deficient, if one assume P as a B site dopant (as shown in our previous work on $Ba_2(In/Sc)_2O_5$), and this can explain the appearance of phosphate impurities. In this work, we have therefore examined cation stoichiometric compositions, assuming the incorporation of P on the B cation site, *i.e.*, $BaCe_{1-y-x}(Y/Yb/In)_yP_xO_{3-y/2+x/2}$, in order to determine whether some phosphate can be incorporated into the perovskite phase. We evaluate the effect of the trivalent cation dopant level on the incorporation of phosphate, and the resultant effect on conductivity and CO_2 stability.

2. Results and Discussion

2.1. $BaCe_{1-y-x}Y_yP_xO_{3-y/2+x/2}$ and $BaCe_{1-y-x}Yb_yP_xO_{3-y/2+x/2}$

Similar to the results of Soares *et al.* on P_2O_5 additions to $BaY_{0.15}Zr_{0.85}O_{2.925}$, we found that for low levels of Y/Yb ($y < 0.2$) it was not possible to introduce significant levels of phosphate [23]. Thus, for example, a composition $BaY_{0.1}Ce_{0.8}P_{0.1}O_3$ showed the presence of small $Ba_{10}(PO_4)_6(OH)_2$ impurities (Figure 1). The presence of such impurities can most probably be related to the need for significant oxide ion vacancies to allow the tetrahedral coordination of phosphate. In agreement with this conclusion, increasing the Y/Yb content to introduce further oxide ion vacancies led to the synthesis of single phase phosphate doped samples. Therefore the results indicate that provided the Y/Yb content is sufficiently high, phosphate can be accommodated into the structure. The powder X-ray diffraction patterns (Figure 2) thus indicated single phase compositions for a range of compounds ($x = 0.05$, $y = 0.2$, 0.25, 0.3; $x = 0.1$, $y = 0.3$) for both Y/Yb doped samples. At higher yttrium and ytterbium contents, $Ba_3Y_4O_9$ and $Ba_3Yb_4O_9$ impurities were formed. The lattice parameters, Table 1, were found to decrease on increased ytterbium content, in agreement with the smaller size of Yb^{3+} compared to Ce^{4+}, and decrease on increased phosphate content in agreement with the smaller size of P^{5+} compared to Ce^{4+}. In the case of Y doping, a similar decrease in cell volume on phosphate doping was observed, but the cell volume also somewhat unexpectedly decreased on increasing Y content, despite the larger size of Y^{3+} *versus* Ce^{4+}. This was attributed to partial substitution of Y onto the Ba site, which was supported by preliminary structural refinements using the X-ray diffraction data. Similar effects have been observed in $BaCe_{1-y}Y_yO_{3-y/2}$ by Wu et al [24]. Such partial substitution of Y on the Ba site would lead to a reduction in the oxide ion vacancy concentration, and likely contribute to a negative effect on the conductivity. It is possible that similar partial substitution on Yb on the Ba site is also occurring for the Yb containing samples. Further structural characterisation using neutron diffraction data is required to get more detailed structural information, in particular regarding the oxide ion sites.

Raman data were collected on all the samples to confirm the presence of phosphate and these showed a band at ~940 cm^{-1}, with selected compositions shown in Figure 3, consistent with the incorporation of phosphate groups into the sample as seen by Shin *et al* [21]. The other bands seen in the Raman spectrum are all indicative of bands associated with yttria doped barium cerates.

The conductivities of all the samples were initially collected in N_2 atmospheres to eliminate any p-type contribution to the conductivity, as has been seen in oxyanion doped $Ba_2(Sc/In)_2O_5$ and $Ba_2Sc_{2-y}Ga_yO_5$, and in dry and wet N_2 atmospheres to observe any protonic contribution to the conductivity [21,22]. The data showed high conductivities with a significant enhancement in wet N_2. This enhanced conductivity in the presence of water vapour is consistent with water incorporation leading to a protonic contribution to the conductivity, Table 2 and Figure 4. Similar conductivities were observed for all samples, with small variations with Y/Yb and phosphate content. The observed conductivities were, however, inferior to the conductivities reported in the literature for Y/Yb doped $BaCeO_3$ without phosphate doping [1,3], suggesting that in this system, the phosphate doping is detrimental to the conductivity, which may be due to partial oxide ion vacancy defect trapping around the phosphate, so as to maintain its tetrahedral coordination. Measurements carried out in dry O_2 showed a conductivity enhancement over the data in dry N_2, which confirms the presence of a p-type

contribution at elevated temperatures (>550 °C) to the conductivity, consistent with the results for $Ba(Ce/Zr)O_3$ systems without phosphate doping (Figure 5). The Y doped samples were analysed further in order to determine the level of water uptake. To hydrate the samples, they were heated up to 800 °C and then slow cooled (0.4 °C/min) to room temperature under flowing wet N_2. The water contents were then determined using TGA analysis, Table 3, showing water contents of up to 0.1 moles per formula unit.

A major concern with yttrium doped $BaCeO_3$ is its instability towards CO_2 atmospheres, as it has a tendency to form $BaCO_3$ when heated in a CO_2 atmosphere at typical fuel cell operating temperatures (500–800 °C) [8]. Phosphate doping had previously been shown to improve the CO_2 stability of $Ba_2M_2O_5$ (M = In, Sc) proton conductors, and therefore the stabilities of these samples were examined by TGA measurements under heating in 1:1 N_2:CO_2, and compared with $BaCe_{0.9}Y_{0.1}O_{2.95}$ [19,21]. The collected data showed that for the Y containing systems there was no improvement in CO_2 stability upon phosphate doping with all compositions showing a similar gain in mass at 450 °C. For the Yb doped samples, there was again little change in stability, although for the higher ytterbium content samples, a small improvement was seen, with the temperature at which the initial mass gain occurred increasing to 500 °C, Figure 6.

2.2. $BaCe_{1-y-x}In_yP_xO_{3-y/2+x/2}$

As for the Y/Yb doped samples, it was necessary to increase the In content to accommodate phosphate. The successfully prepared $BaCe_{1-y-x}In_yP_xO_{3-y/2+x/2}$ phases are listed in Table 4 with the XRDs shown in Figure 7. The cell parameters were obtained, Table 5, and the cell volumes show a general decrease upon increasing indium and phosphate content in agreement with In^{3+} and P^{5+} having a smaller ionic radius than Ce^{4+}. Raman data confirmed the incorporation of phosphate, with all samples showing bands at ~940 cm^{-1}, Figure 8.

The conductivities of these In doped samples were lower than those obtained for $BaCe_{1-y-x}Y/Yb_yP_xO_{3-y/2+x/2}$, Table 5, and the conductivities were furthermore lowered on increasing phosphate content. As for the Y,Yb doped samples, these samples showed enhanced conductivities in wet N_2 and dry O_2 consistent with a protonic and p-type conductivity contribution respectively, Figures 9 and 10.

The water contents of hydrated samples were determined by TGA measurements and these data (Table 6) showed that the levels of water incorporation were lower than seen for the yttrium analogues, which may explain the lower conductivities observed. In particular it would suggest that less oxide ion vacancies are available for water incorporation, and hence would imply a greater degree of oxide ion vacancy defect trapping.

The relative CO_2 stabilities were also measured and in this case there appeared to be an improvement in the CO_2 stability on phosphate doping, with the temperature at which the initial mass gain occurred increasing from 450 to 575 °C, Table 6. This indicated that while phosphate doping lowers the conductivity in $BaCe_{1-y-x}In_yP_xO_{3-y/2+x/2}$ it does appear to improve the chemical stability towards CO_2 as similarly seen for $Ba_2In_2O_5$ and $Ba_2Sc_2O_5$ [19,21]. At present, it is not clear why there is an improvement in the CO_2 stability for the In containing samples, but not for the Y, Yb containing samples. Further work would be required to clarify this, but it could be affected by different degrees of

local order between the trivalent dopants and the phosphate group, and in this respect computer modeling studies may provide some insight.

Table 1. Cell parameter data for orthorhombic $BaCe_{1-y-x}(Y/Yb)_yP_xO_{3-y/2+x/2}$.

Sample (nominal composition)	Unit cell parameters (Å)			Unit cell volume (Å^3)
	a	b	c	
$BaCe_{0.8}Y_{0.2}O_{2.9}$	8.9137(9)	6.1815(6)	6.1793(7)	340.48(8)
$BaCe_{.75}Y_{0.2}P_{0.05}O_{2.925}$	8.7431(3)	6.1998(2)	6.2186(2)	337.09(2)
$BaCe_{0.7}Y_{0.25}P_{0.05}O_{2.9}$	8.7363(3)	6.1978(2)	6.2188(2)	336.73(2)
$BaCe_{0.65}Y_{0.3}P_{0.05}O_{2.875}$	8.7302(4)	6.1969(3)	6.2191(2)	336.46(3)
$BaCe_{0.6}Y_{0.3}P_{0.1}O_{2.9}$	8.7240(5)	6.1856(3)	6.2061(3)	334.90(3)
$BaCe_{.75}Yb_{0.2}P_{0.05}O_{2.925}$	8.7267(6)	6.1815(4)	6.2113(4)	335.06(5)
$BaCe_{0.7}Yb_{0.25}P_{0.05}O_{2.9}$	8.718(1)	6.174(1)	6.213(1)	334.4(1)
$BaCe_{0.65}Yb_{0.3}P_{0.05}O_{2.875}$	8.6973(5)	6.1714(4)	6.1964(3)	332.59(4)
$BaCe_{0.6}Yb_{0.3}P_{0.1}O_{2.9}$	8.697(1)	6.1578(6)	6.1892(6)	321.49(7)

Table 2. Conductivity data for $BaCe_{1-y}Y_{y-x}P_xO_{3-y/2+x/2}$.

Sample (nominal composition)	Conductivity (S cm^{-1})			
	500 °C		800 °C	
	Dry N_2	Wet N_2	Dry N_2	Wet N_2
$BaCe_{0.8}Y_{0.2}O_{2.9}$	3.7×10^{-3}	3.7×10^{-3}	2.4×10^{-2}	1.9×10^{-2}
$BaCe_{.75}Y_{0.2}P_{0.05}O_{2.925}$	1.4×10^{-3}	1.7×10^{-3}	4.9×10^{-3}	5.9×10^{-3}
$BaCe_{0.7}Y_{0.25}P_{0.05}O_{2.9}$	1.4×10^{-3}	2.1×10^{-3}	6.0×10^{-3}	7.3×10^{-3}
$BaCe_{0.65}Y_{0.3}P_{0.05}O_{2.875}$	2.0×10^{-3}	2.5×10^{-3}	6.8×10^{-3}	8.2×10^{-3}
$BaCe_{0.6}Y_{0.3}P_{0.1}O_{2.9}$	1.2×10^{-3}	1.4×10^{-3}	3.3×10^{-3}	4.1×10^{-3}
$BaCe_{.75}Yb_{0.2}P_{0.05}O_{2.925}$	8.6×10^{-4}	2.0×10^{-3}	6.4×10^{-3}	7.2×10^{-3}
$BaCe_{0.7}Yb_{0.25}P_{0.05}O_{2.9}$	1.7×10^{-3}	2.5×10^{-3}	1.2×10^{-2}	1.2×10^{-2}
$BaCe_{0.65}Yb_{0.3}P_{0.05}O_{2.875}$	8.5×10^{-4}	1.6×10^{-3}	4.3×10^{-3}	4.6×10^{-3}
$BaCe_{0.6}Yb_{0.3}P_{0.1}O_{2.9}$	4.4×10^{-4}	6.3×10^{-4}	2.6×10^{-3}	2.8×10^{-3}

Table 3. Water content for $BaCe1_{-y-x}Y_yP_xO_{3-y/2+x/2}$.

Sample (nominal composition)	Moles of water per formula unit
$BaCe_{0.8}Y_{0.2}O_{2.9}$	0.10(1)
$BaCe_{.75}Y_{0.2}P_{0.05}O_{2.925}$	0.03(1)
$BaCe_{0.7}Y_{0.25}P_{0.05}O_{2.9}$	0.11(1)
$BaCe_{0.65}Y_{0.3}P_{0.05}O_{2.875}$	0.09(1)
$BaCe_{0.6}Y_{0.3}P_{0.1}O_{2.9}$	0.05(1)

Table 4. Cell parameter data for orthorhombic $BaCe_{1-y-x}In_yP_xO_{3-y/2+x/2}$.

Sample (nominal composition)	Unit cell parameters (Å)			Unit cell volume (Å^3)
	a	b	c	
$BaCe_{0.8}In_{0.2}O_{2.9}$	6.2094(2)	6.1898(2)	8.7204(3)	335.17(2)
$BaCe_{0.75}In_{0.2}P_{0.05}O_{2.925}$	6.1940(1)	6.1700(1)	8.7135(2)	333.01(2)
$BaCe_{0.7}In_{0.25}P_{0.05}O_{2.9}$	6.1587(2)	6.1796(1)	8.6999(3)	331.11(2)
$BaCe_{0.65}In_{0.3}P_{0.05}O_{2.875}$	6.1445(2)	6.1632(2)	8.6892(3)	329.06(1)
$BaCe_{0.6}In_{0.3}P_{0.1}O_{2.9}$	6.1285(4)	6.1496(3)	8.6692(5)	326.73(2)

Table 5. Conductivity data for $BaCe_{1-y-x}In_yP_xO_{3-y/2+x/2}$.

Sample (nominal composition)	Conductivity (S cm^{-1})			
	500 °C		800 °C	
	Dry N_2	Wet N_2	Dry N_2	Wet N_2
$BaCe_{0.8}In_{0.2}O_{2.9}$	7.4×10^{-5}	5.3×10^{-4}	1.6×10^{-3}	2.4×10^{-3}
$BaCe_{0.75}In_{0.2}P_{0.05}O_{2.925}$	1.8×10^{-5}	2.5×10^{-4}	2.8×10^{-4}	8.7×10^{-4}
$BaCe_{0.7}In_{0.25}P_{0.05}O_{2.9}$	1.4×10^{-4}	2.4×10^{-4}	1.3×10^{-3}	1.3×10^{-3}
$BaCe_{0.65}In_{0.3}P_{0.05}O_{2.875}$	2.1×10^{-5}	2.4×10^{-4}	6.2×10^{-4}	1.2×10^{-3}
$BaCe_{0.6}In_{0.3}P_{0.1}O_{2.9}$	8.5×10^{-6}	1.1×10^{-4}	2.3×10^{-4}	4.7×10^{-4}

Table 6. Water content and temperature for uptake of CO_2 for $BaCe_{1-y}In_yP_xO_{3-y/2+x/2}$.

Sample (nominal composition)	Moles of water per formula unit	Temperature of CO_2 mass gain (°C)
$BaCe_{0.8}In_{0.2}O_{2.9}$	0.04(1)	450
$BaCe_{0.75}In_{0.2}P_{0.05}O_{2.925}$	0.03(1)	525
$BaCe_{0.7}In_{0.25}P_{0.05}O_{2.9}$	0.03(1)	550
$BaCe_{0.65}In_{0.3}P_{0.05}O_{2.875}$	0.02(1)	550
$BaCe_{0.6}In_{0.3}P_{0.1}O_{2.9}$	0.04(1)	575

Figure 1. XRD pattern for attempted synthesis of "$BaCe_{0.8}Y_{0.1}P_{0.1}O_3$" with $Ba_{10}(PO_4)_6(OH)_2$ impurity peaks indicated.

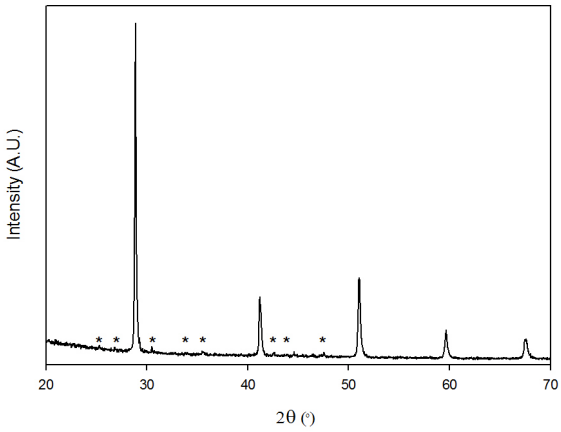

Figure 2. XRD patterns for $BaCe_{1-y}(Y/Yb)_yP_xO_{3-y/2+x/2}$ with inset showing $Ba_3Y_4O_9$ and $Ba_3Yb_4O_9$ impurity phase for attempted synthesis of $BaCe_{0.5}Y_{0.4}P_{0.1}O_{2.8}$ and $BaCe_{0.5}Yb_{0.4}P_{0.1}O_{2.8}$.

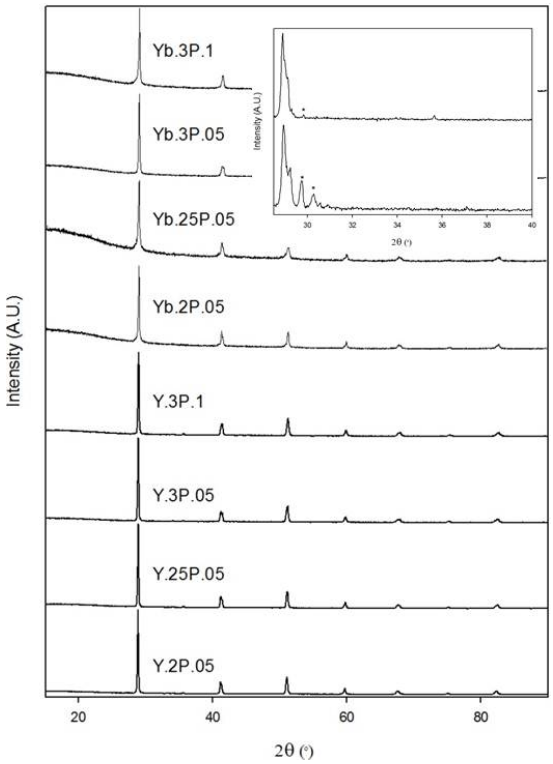

Figure 3. Raman spectra of $BaCe_{0.75}Y_{0.2}P_{0.05}O_{2.925}$ and $Ba_2Ce_{0.6}Y_{0.3}P_{0.1}O_{2.9}$ with band showing the presence of phosphate indicated.

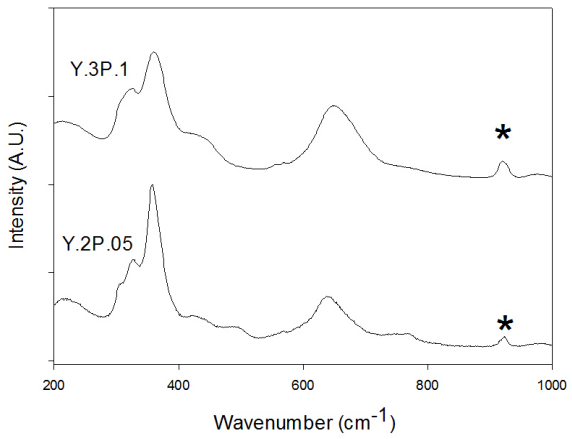

Figure 4. Conductivity data between 350 °C and 800 °C for $BaCe_{0.75}Y_{0.2}P_{0.05}O_{2.925}$ (circle) and $BaCe_{0.65}Y_{0.3}P_{0.05}O_{2.875}$ (square) in dry (empty) and wet (filled) N_2.

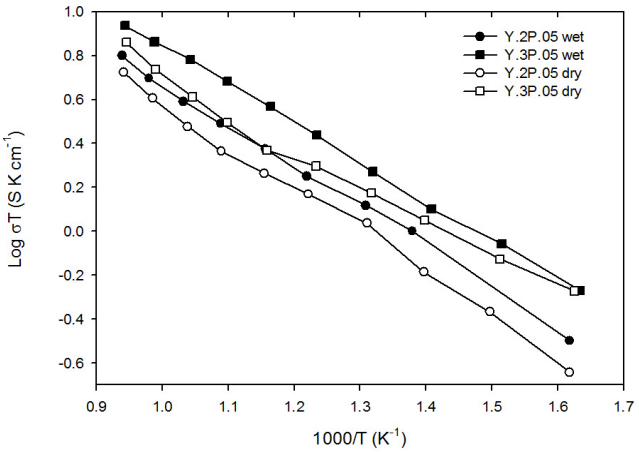

Figure 5. Conductivity data between 400 °C and 800 °C for $BaCe_{0.65}Y_{0.3}P_{0.05}O_{2.875}$ in dry N_2 (filled circle) and dry O_2 (empty circle).

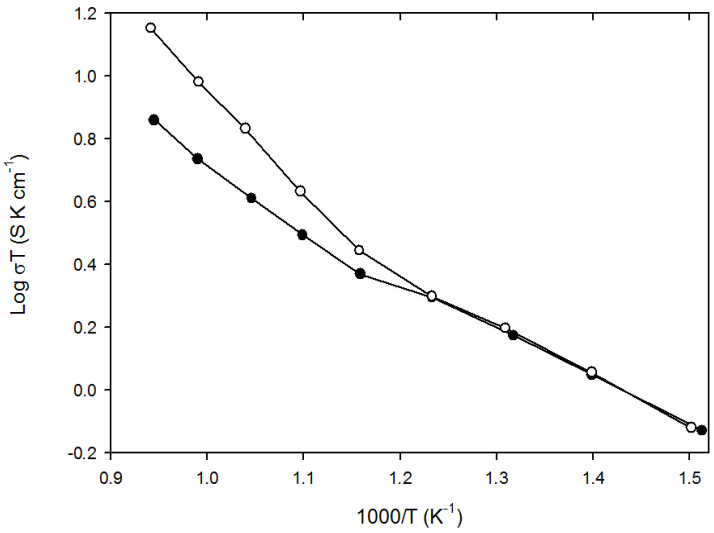

Figure 6. TG profiles (10 °C min^{-1} to 1000 °C in 1:1 CO_2 and N_2 mixture) for (**a**) $BaCe_{0.6}Y_{0.3}P_{0.1}O_{2.9}$ and (**b**) $BaCe_{0.6}Yb_{0.3}P_{0.1}O_{2.9}$.

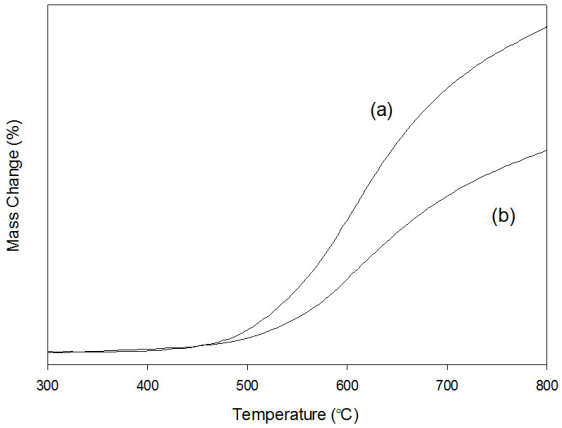

Figure 7. XRD patterns for $BaCe_{1-y-x}In_yP_xO_{3-y/2+x/2}$ (x = 0.05, y = 0.2, 0.25, 0.3; x= 0.1, y = 0.3).

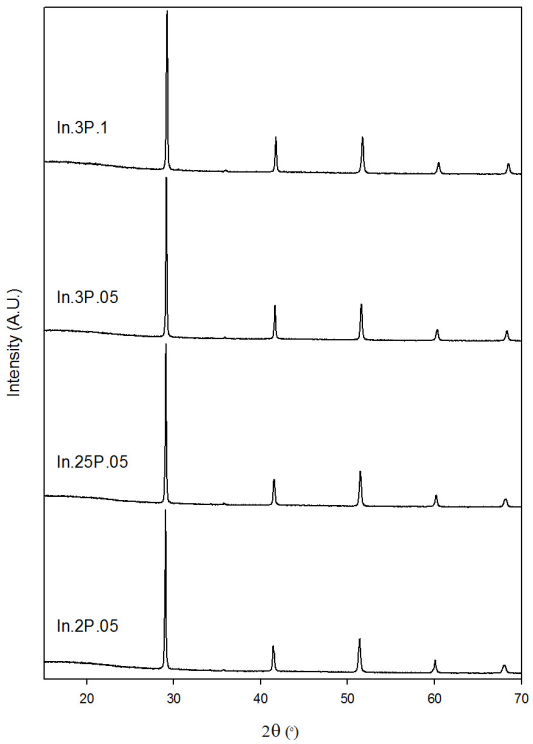

Figure 8. Raman spectra of $BaCe_{0.75}In_{0.2}P_{0.05}O_{2.925}$ and $BaCe_{0.6}In_{0.3}P_{0.1}O_{2.9}$ with band showing the presence of phosphate indicated.

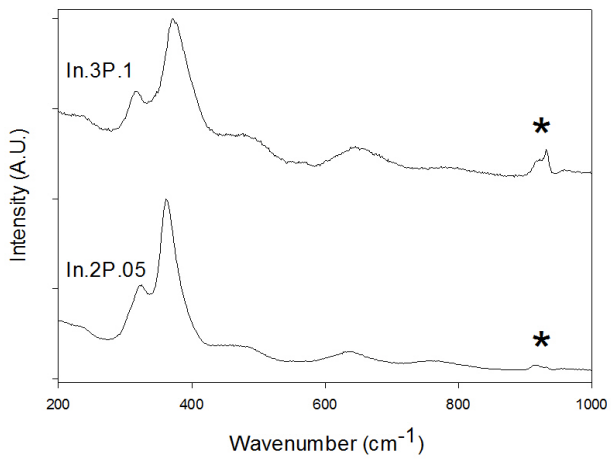

Figure 9. Conductivity data between 350 °C and 800 °C for $BaCe_{0.75}In_{0.2}P_{0.05}O_{2.925}$ (circle) and $BaCe_{0.65}In_{0.3}P_{0.05}O_{2.875}$ (square) in dry (empty) and wet (filled) N_2.

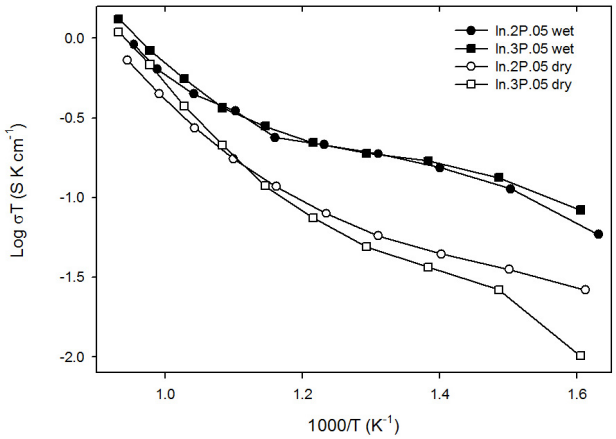

Figure 10. Conductivity data between 500 °C and 800 °C for $BaCe_{0.65}In_{0.3}P_{0.05}O_{5.875}$ in dry N_2 (filled circle) and dry O_2 (empty circle).

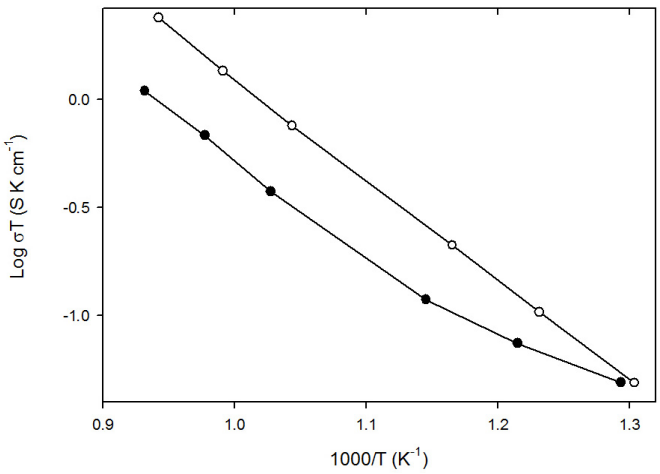

3. Experimental Section

High purity $BaCO_3$, CeO_2, Y_2O_3, In_2O_3, Yb_2O_3 and $NH_4H_2PO_4$ were used to prepare $BaCe_{1-y-x}Y_yP_xO_{3-y/2+x/2}$, $BaCe_{1-y-x}In_yP_xO_{3-y/2+x/2}$ and $BaCe_{1-y-x}Yb_yP_xO_{3-y/2+x/2}$ samples. A small (3%) excess of $BaCO_3$ was employed, in order to overcome Ba loss at elevated temperatures as has been seen in other studies synthesising similar Ba containing phases [18,19]. The powders were intimately ground and heated initially to 1000 °C for 12 h. They were then ball-milled (350 rpm for 1 h, Fritsch Pulverisette 7 Planetary Mill) and reheated to 1100 °C for 12 h. The resulting powders were then ball-milled (350 rpm for 1 h, Fritsch Pulverisette 7 Planetary Mill) a second time and pressed as pellets (1.3 cm diameter) and sintered at 1400 °C for 12 h. The pellets were covered in sample powder and the crucible was covered with a lid to limit the amount of Ba loss during the sintering process. Powder X-ray diffraction (Bruker D8 diffractometer with Cu $K\alpha_1$ radiation) was used to demonstrate phase purity as well as for preliminary structure determination. For the latter, the GSAS suite of programs was used [25].

Raman spectroscopy measurements were made in order to provide further evidence for the successful incorporation of phosphate. These measurements utilised a Renishaw inVia Raman microscope with excitation using a Cobolt Samba CW 532 nm DPSS Laser.

The CO_2 stabilities of samples were determined using thermogravimetric analysis (Netzsch STA 449 F1 Jupiter Thermal Analyser). Samples were heated at 10 °C min^{-1} to 1000 °C in a 1:1 CO_2 and N_2 mixture to determine at what temperature CO_2 incorporation occurred.

The water contents of hydrated samples were determined from thermogravimetric analysis (Netzsch STA 449 F1 Jupiter Thermal Analyser). Samples were heated at 10 °C min^{-1} to 1000 °C in N_2, and the water content was determined from the observed mass loss.

For the conductivity measurements, the sintered pellets (>80% theoretical) were coated with Pt paste, and then heated to 800 °C for 1 hour to ensure bonding to the pellet. Conductivities were then measured by AC impedance measurements (Hewlett Packard 4192A impedance analyser) in the range from 0.1 to 1.3 × 10^3 kHz. Measurements were made in dry N_2 and wet N_2 (in which the gas was bubbled at room temperature through water) to identify any protonic contribution to the conductivity. Measurements were also made in dry O_2 to determine if there was a p-type electronic contribution to the conductivity. The impedance spectra typically showed a single broad semicircle, corresponding to overlapping of bulk and grain boundary components. The total resistance was determined by the low frequency intercept of this semicircle. Attempts to increase the pellet density by higher temperature sintering were unsuccessful, with such heat treatments leading to evidence for Ba loss and insignificant improvements in densities.

4. Conclusions

The results demonstrate that it is possible to dope phosphate onto the B-cation site in Y,Yb, In doped $BaCeO_3$, although it was necessary to increase the trivalent dopant content to at least 20% to achieve this, which can be explained by the need for sufficient oxide ion vacancies to allow for the accommodation of tetrahedral P^{5+}. The results showed that this doping strategy leads to an improvement to the CO_2 stability for $BaCe_{1-y-x}In_yP_xO_{3-y/2+x/2}$, although for the comparable Y, Yb

doped samples there was little improvement in this respect. Conductivities for all samples were lower than literature reports for such samples without phosphate doping. This may be related both to problems with achieving fully dense pellets for these phosphate doped samples, along with the influence of trapping of oxide ion vacancies around P^{5+} to achieve the required tetrahedral coordination for the phosphate group. The results, nevertheless, highlight the potential of perovskites to accommodate oxyanions.

Acknowledgments

We would like to express thanks to EPSRC (grant EP/I003932) for funding. The Bruker D8 diffractometer, Renishaw inVia Raman microscope, and Netzsch STA 449 F1 Jupiter Thermal Analyser used in this research were obtained through the Science City Advanced Materials project: Creating and Characterising Next generation Advanced Materials project, with support from Advantage West Midlands (AWM) and part funded by the European Regional Development Fund (ERDF).

Conflicts of Interest

The authors declare no conflict of interest.

References

1. Kreuer, K.D. Proton-conducting oxides. *Annu. Rev. Mater. Res.* **2003**, *33*, 333–359.
2. Goodenough, J.B. Oxide-ion electrolytes. *Annu. Rev. Mater. Res.* **2003**, *33*, 91–128.
3. Orera, A.; Slater, P.R. New Chemical Systems for Solid Oxide Fuel Cells. *Chem. Mater.* **2010**, *22*, 675–690.
4. Norby, T. Solid-state protonic conductors: Principles, properties, progress and prospects. *Solid State Ionics* **1999**, *125*, 1–11.
5. Iwahara, H.; Uchida, H.; Ono, K.; Ogaki, K. Proton conduction in sintered oxides based on $BaCeO_3$. *J. Electrochem. Soc.* **1988**, *135*, 529–533.
6. Yajima, T.; Kazeoka, K.; Yogo, T.; Iwahara, H. Proton conduction in sintered oxides based on $CaZrO_3$. *Solid State Ionics* **1991**, *47*, 271–275.
7. Iwahara, H.; Yajima, T.; Hibino, T.; Ozaki, K.; Suzuki, H. Protonic conduction in calcium, strontium and barium zirconates. *Solid State Ionics* **1993**, *61*, 65–69.
8. Scholten, M.J.; Schoonman, J.; van Miltenburg, J.C.; Oonk, H.A.J. Synthesis of strontium and barium cerate and their reaction with carbon dioxide. *Solid State Ionics* **1993**, *61*, 83–91.
9. Babilo, P.; Haile, S.M. Enhanced sintering of yttrium-doped barium zirconate by addition of ZnO. *J. Am. Ceram. Soc.* **2005**, *88*, 2362–2368.
10. Tao, S.; Irvine, J.T.S. Conductivity studies of dense yttrium-doped $BaZrO_3$ sintered at 1325 degrees C. *J. Solid State Chem.* **2007**, *180*, 3493–3503.
11. Ryu, K.H.; Haile, S.M. Chemical stability and proton conductivity of doped $BaCeO_3$-$BaZrO_3$ solid solutions. *Solid State Ionics* **1999**, *125*, 355–367.

12. Katahira, K.; Kohchi, Y.; Shimura, T.; Iwahara, H. Protonic conduction in Zr-substituted $BaCeO_3$. *Solid State Ionics* **2000**, *138*, 91–98.
13. Goodenough, J.B.; Ruizdiaz, J.E.; Zhen, Y.S. Oxide-ion conduction in $Ba_2In_2O_5$ and $Ba_3In_2CeO_8$, $Ba_3In_2HFO_8$, or $Ba_3In_2ZrO_8$. *Solid State Ionics* **1990**, *44*, 21–31.
14. Rolle, A.; Vannier, R.N.; Giridharan, N.V.; Abraham, F. Structural and electrochemical characterisation of new oxide ion conductors for oxygen generating systems and fuel cells. *Solid State Ionics* **2005**, *176*, 2095–2103.
15. Quarez, E.; Noirault, S.; Caldes, M.T.; Joubert, O. Water incorporation and proton conductivity in titanium substituted barium indate. *J. Power Sources* **2010**, *195*, 1136–1141.
16. Karlsson, M.; Matic, A.; Knee, C.S.; Ahmed, I.; Eriksson, S.G.; Borjesson, L. Short-range structure of proton-conducting perovskite $BaIn_xZr_{1-x}O_{3-x/2}$ (x = 0–0.75). *Chem. Mater.* **2008**, *20*, 3480–3486.
17. Shin, J.F.; Hussey, L.; Orera, A.; Slater, P.R. Enhancement of the conductivity of $Ba_2In_2O_5$ through phosphate doping. *Chem. Commun*. **2010**, *46*, 4613–4615.
18. Shin, J.F.; Apperley, D.C.; Slater, P.R. Silicon Doping in $Ba_2In_2O_5$: Example of a Beneficial Effect of Silicon Incorporation on Oxide Ion/Proton Conductivity. *Chem. Mater*. **2010**, *22*, 5945–5948.
19. Shin, J.F.; Orera, A.; Apperley, D.C.; Slater, P.R. Oxyanion doping strategies to enhance the ionic conductivity in $Ba_2In_2O_5$. *J. Mater. Chem*. **2011**, *21*, 874–879.
20. Shin, J.F.; Slater, P.R. Enhanced CO_2 stability of oxyanion doped $Ba_2In_2O_5$ systems co-doped with La, Zr. *J. Power Sources* **2011**, *196*, 8539–8543.
21. Shin, J.F.; Joubel, K.; Apperley, D.C.; Slater, P.R. Synthesis and characterization of proton conducting oxyanion doped $Ba_2Sc_2O_5$. *Dalton Trans.* **2012**, *41*, 261–266.
22. Smith, A.D.; Shin, J.F.; Slater, P.R. Synthesis and characterization of oxyanion (phosphate, sulphate) doped $Ba_2Sc_{2-y}Ga_yO_5$. *J. Solid State Chem.* **2013**, *198*, 247–252.
23. Soares, H.S.; Zhang, X.; Antunes, I.; Frade, J.R.; Mather, G.C.; Fagg, D.P. Effect of phosphorus additions on the sintering and transport properties of proton conducting $BaZr_{0.85}Y_{0.15}O_{3-delta}$. *J. Solid State Chem.* **2012**, *191*, 27–32.
24. Wu, J.; Li, L.P.; Espinosa, W.T.P.; Haile, S.T. Defect chemistry and transport properties of $Ba_xCe_{0.85}M_{0.15}O_{3-delta}$. *J. Mater. Res.* **2004**, *19*, 2366–2376.
25. Larson, A.C.; von Dreele, R.B. *General Structure Analysis System (GSAS)*; Report. No LAUR 86–748; Los Alamos National Laboratory: Los Alamos, NM, USA, 2004.